Astronomy & Astrophysics manuscript no.
(will be inserted by hand later)

Magnetic fields at OH Maser Sources in W49N

Mendoza-Torres J.E. 1[1], Goss W.M. [2], Streb S. [3], Deshpande A.A. [4], Laskar T. [5],[6]

[1] Instituto Nacional de Astrofísica, Optica y Electrónica, Apartado Postal 51 y 216, Puebla, Pue., Z.P. 72000, México

[2] NRAO

[3] Salpointe Catholic High School, Tucson, AZ

[4] Raman Research Institute, Bangalore, India

[5] Department of Physics, Cavendish Laboratory, University of Cambridge, JJ Thomson Avenue, Cambridge CB3 0HE, UK

[6] Space Telescope Science Institute, 3700 San Martin Dr., Baltimore, MD 21218, USA

Received ...

Abstract. We have analyzed VLBA observations of W49N at the OH maser frequencies 1612 MHz, 1665 MHz and 1667 MHz. More than two hundred masers spots were detected. For all of them the Major axis, the minor axis, the principal axis (PA), the central velocity and the linewidth were measured. The deconvolved angular size of the major axis range from 30 to 70 mas, the minor axis from 20 to 50 and the PA takes values from 70° to 130°. At the same field of the observed OH masers there are seven UC HII regions. Some of OH maser spots are cospatial to UC HII regions but many other are not. Other spots are in zones with no HII regions. It is found that subsets of OH spots are forming structures, among them a small and a large arc, a jet and a ring. The magnetic field at the OH sources is estimated based on Zeeman pairs. The magnetic fields at the small arc, at the jet and at the ring show a regular behaviour with smooth variations but at the large arc the field varies aleatory. Although the OH spots are spread over a wide field and located at very different structures their PAs have similar values to each other.

Key words. Masers: OH, Masers: Zeeman

Send offprint requests to: Mendoza-Torres J.E.

mend@inaoep.mx

1. Introduction

W49N is a Star-Forming-Region (SFR) located at a distance of 11.4 kpc (Gwinn et al. 1992) at a low galactic latitude, close to the disc. It is characterized by the presence of a number of HII regions (Dreher et al. (1984) and De Pree et al. (2000)) and, in a smaller scale, by H_2O maser spots tracing two oppositely directed outflows. The HII regions, initially identified by Dreher et al. (1984) as ultracompact (UC) and now referred to as hyper-compact (HC) H II regions (Kurtz 2000) because are about one order of magnitude smaller that UC HII regions (Kurtz & Franco 2002), are thought to be driven by O stars, making this region one of the sites at our Galaxy with active formation of massive stars.

Since the HC H II regions are typically about two orders of magnitude denser than UC HII regions, the W49N region seems to have conditions (De Pree et al. 2000) where the HII regions reach the equilibrium with the environment at shorter distances than typical UC HII regions (Wood & Churchwell 1989). OH masers have been detected at W49N. The presence of O stars create an ideal scenario to switch-on OH maser emission thus making it a source reach in OH maser spots that could give an insight into the environment of the HC HII regions. Also, estimates of the magnetic field have been done for OH maser sources (Fish et al. 2006). Such estimates are clue to have an idea of the role that magnetic fields could play in such particular regions.

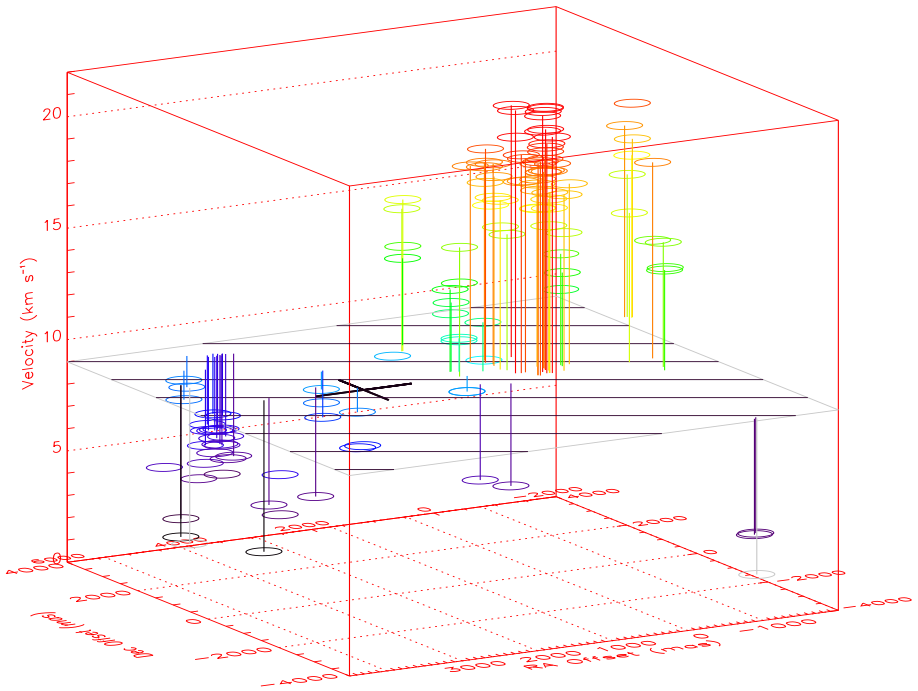

Fig. 1. 3D scatter plot for the spots at 1667 MHz, a plane at a velocity of 9 km s^{-1}, which is around the central velocity, is plotted as reference. The color of each ellipse is proportional to its velocity, purple is for blue-shifted and red for red-shifted.

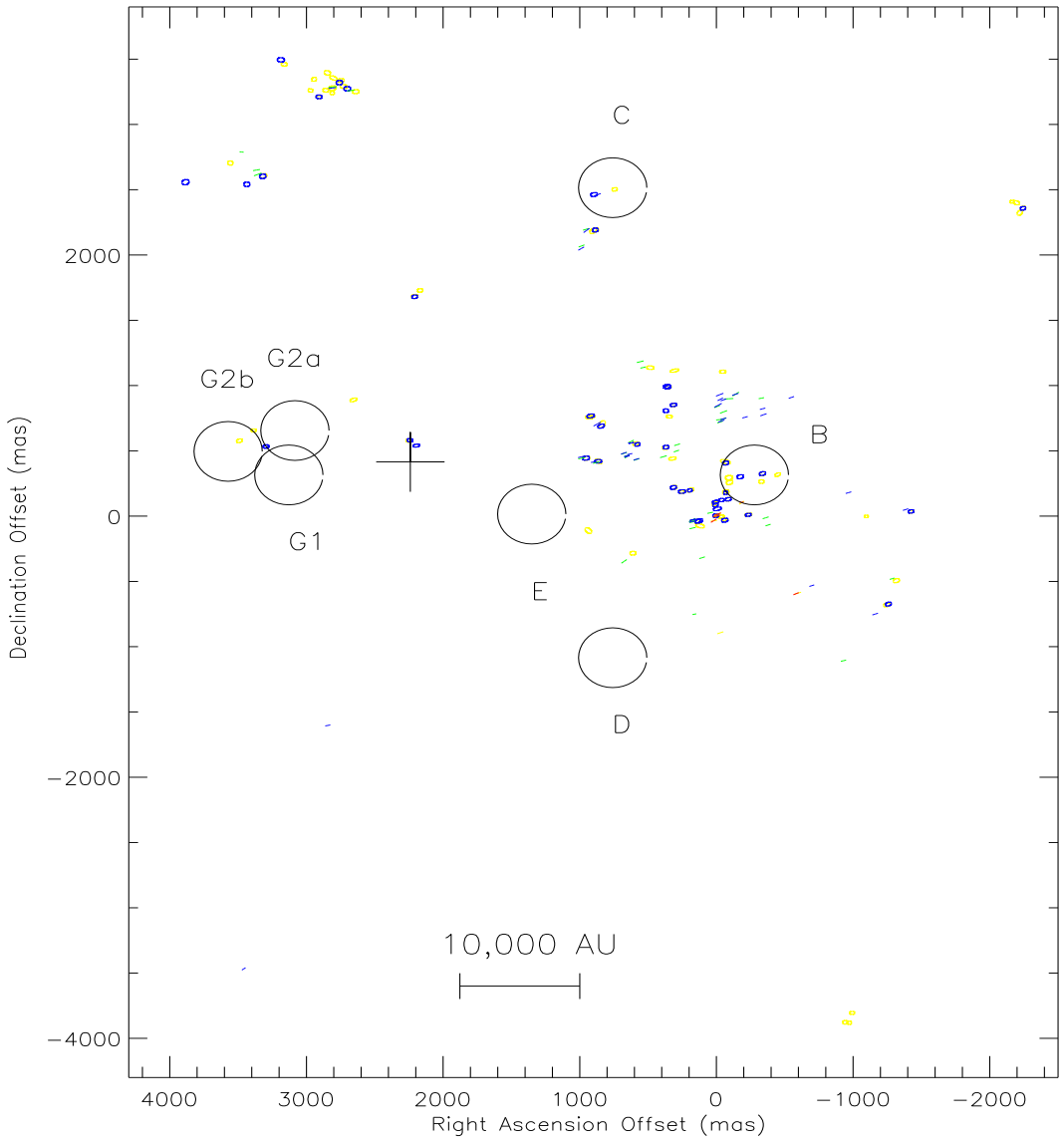

Fig. 2. Distribution of W49N spots. Yellow ellipses are for LCP 1667 MHz spots, blue ellipses for RCP 1667 MHz spots. The ellipses are of the actual sizes and are oriented at the PA observed in each case. The extension and orientation of the bars denote, respectively, the Major axis and the PA of the spots as follows, LCP 1665 MHz (green bars), RCP 1665 MHz (blue bars), LCP 1612 MHz (yellow bars), RCP 1612 MHz (red bars). The circles denote the HII regions C, E, B anf G of Dreher et al. (1984) and $G1$ and $G2$ of De Pree et al. (2000). The CE of Gwinn et al. (1992) is denoted by a *cross*.

2. Observations and data analysis

The 1667.35903 MHz (hereafter 1667 MHz), 1665.4018 MHz (hereafter 1665 MHz) and 1612.23101 MHz (hereafter 1612 MHz) transitions were observed toward W49N with the VLBA on 2005 October 6.

The reference coordinates are RA=19 10 13.2091 and Dec=09 06 12.485. Left Circular Polarization (LCP) and Right Circular Polarization (RCP) are observed simultaneously in about 240 spectral channels with a resolution of 0.1 km s^{-1} in a range of about 22

km s^{-1}. The beam size is about 20 mas by 15 mas at a position angle of 84 degrees. The galactic plane is at a position angle of 30°.

We have detected 208 spots and all have an elliptical shape whose major axis (further denoted when necessary as M), minor axis (also further denoted when necessary as m) and the Principal Angle (PA) are estimated using the JMFIT AIPS routine (Tables 2-7). The XGAUSS routine was used to estimate the center and width of the spectral line for each spot as given at the same Tables.

3. Spatial distribution of spots

A total of 208 spots were detected. At the three frequencies more spots at LCP than at RCP were detected (Table 1). The major axis of the spots takes values between 30 and 70 mas, which for a distance of 11.4 kpc corresponds to 350 and 800 AU.

Table 1. Amounts of detected spots

ν	L	R	L+R
1667	76	44	120
1665	42	35	76
1612	6	5	11

The OH spots are distributed on a field of about 6 ″ (Fig.1), that corresponds to $7{\cdot}10^4$ AU. Two main groups are seen nearly aligned in Nort-East to South-West direction (Fig.2). OH spots have been previously observed with a larger uncertainty but at the same field that the spots reported here (Kent and Mutel, 1982). H_2O spots have been observed in a more compact distribution that is lengthen in East-West direction (Gwinn et al, 1992) and that traces flows from a Center of Expansion (CE) (denoted by a *cross* in Fig.1 and Fig.2). Eastern H_2O spots are slightly to the north respect the Western ones.

The velocities of the OH spots that lie near the CE on the West side have velocities ≤ 9 km s^{-1} and the spots near CE on the East side have velocities ≥ 9 km s^{-1}. Coincidentally, the middle of the range of velocities of the spots becomes about 9 km s^{-1}. In Fig.1 a plane is plotted at this velocity. It may be seen that most of the spots with blue velocities, respect 9 km s^{-1}, are located at the West, while red shifted spots predominantly appear at the East. This behaviour is similar to that observed by Kent and Mutel (1982) also for OH spots. However, the H_2O spots show a distinct behavior; the East H_2O spots are red shifted and the West are blue shifted. It means, the H_2O velocities are of the opposite sign respect the OH ones. The interpretation of this result is not straightforward

but could due to large inflows that influence the OH spots velocities and outflows at the shorter scale of the H_2O spots.

In Fig. 2 the locations of the observed maser spots are denoted by small ellipses and small bars, the locations of HII regions observed by Dreher et al. (1984) and De Pree et al. (2000) are denoted by circles.

4. Spots forming structures

It has beenn found that some groups of spots seem to trace some particular structures.

4.1. Small arc

A subset of six spots (three at LCP and three at RCP 1667 MHz) form a small arc. The yellow ellipses denote the LCP and blue the RCP 1667 MHz spots. The bars are for 1665 MHz (green for LCP and blue for RCP) and 1612 MHz spots (yellow for LCP and red for RCP). A circle is fitted to the spots (small dashed circle of Fig.3) and the cross on the East corresponds to the center of the circle. The six spots form Zeeman pairs. The estimated magnetic fields are given in Table 10. A velocity gradient takes place from East to West, it may be seen in Fig. 5 where the distance is referenced to the Eastern spot.

4.2. Large arc

A subset of spots forms an arc of about 0.5 sec length. At the West and at the South-West of the arc some spots are located in a sequence to the West and to the South-West as if they would be in a filament. The distribution of these spots (including those outside the drawn field) are roughly aligned as going away from the gaps in the arc Fig.2.

The northern half of the arc seems to trace a velocity gradient going from 16.1 km^{-1} at the North to 20.7 km^{-1} at the South. The large dashed circle of Fig.3 fits well to the spots at the north part of the large arc. The center of this circle is at the West of the center of the small dashed circle.

4.3. Jet

A subset of 1665 and 1667 MHz spots is roughly distributed following a straight line, a that plotted in Fig.3. The jet has a length of 700 mas ($\sim$ 8000 AU). The velocity of the LCP 1667 MHz spots goes from about 15.2 $km\ s^{-1}$ at the South to 18.7 $km\ s^{-1}$ (at 550 mas North $\sim$ 6300 AU) where the velocity has a turnover to smaller values. The behaviour of the velocity along these spots indicates that they are located in a jet. The velocity of the RCP spots is smaller relative the LCP one. This is due to the presence of magnetic fields (Fish et al. 2006) and will be below discussed.

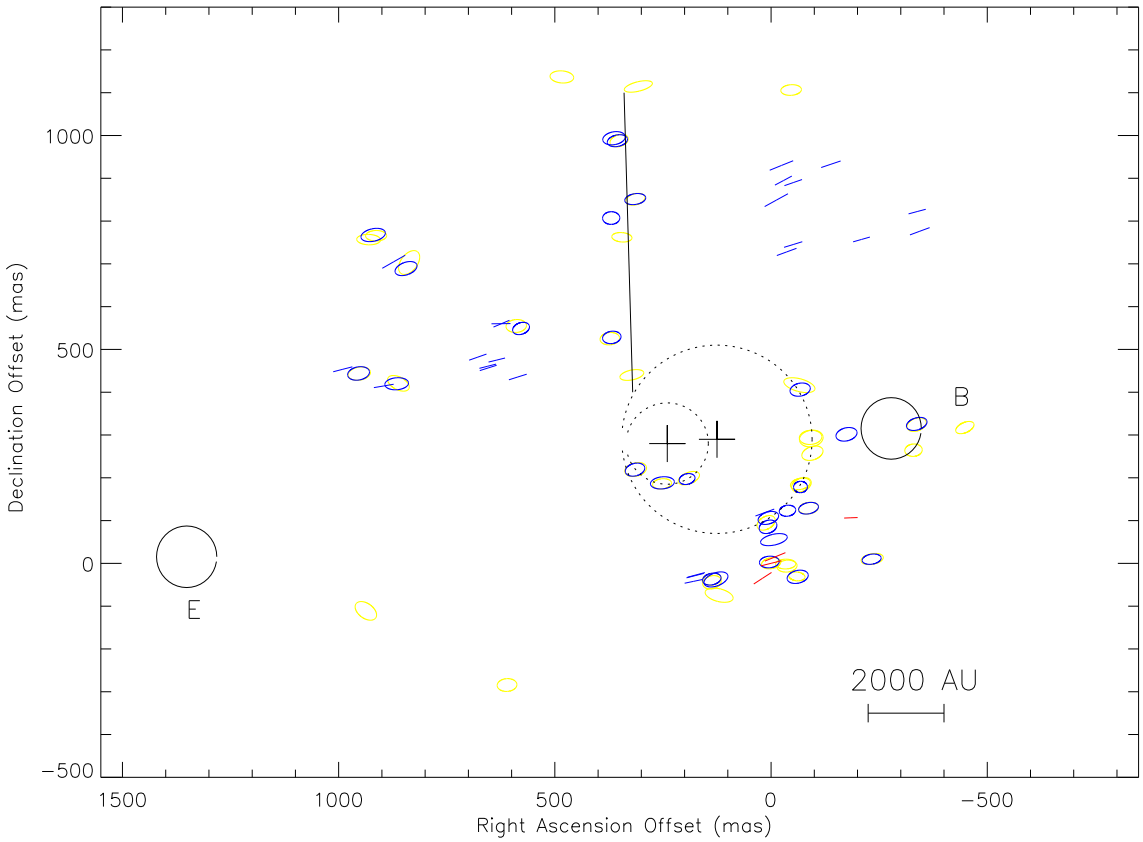

Fig. 3. A subset of spots at the Western side (right hand side) of Fig.2. Yellow ellipses are for LCP 1667 MHz spots, blue ellipses for RCP 1667 MHz spots. The ellipses are oriented at the PA observed in each case, and their sizes are the actual ones. The extension and orientation of the bars are as in Fig.2. The dashed circles indicate arcs formed by spots. The velocity of the spots that lie at the large circle increases clockwise, i.e. from North (16.1 km s^{-1} LCP 1667 MHz) to South (20.7 km s^{-1} LCP 1667 MHz). Also the velocity of the spots at the small arc grows clockwise, from West (18.6 km s^{-1} LCP 1667 MHz) to East (20.8 km s^{-1} LCP 1667 MHz).

4.4. Ring

Another subset of 1667 MHz spots forms a ring whose diameter is about 800 AU. Each spot at the ring appears at several channels. The location of some spots differs from one channel to other. The PA of the five Eastern spots of the ring has a tendency to be tangent to the ring but at the same time does not considerably differs from the orientation of the other spots at the field. In general, the positions of the maser spots change from one channel to other. In a subset of the spots at the West side the shift is considerably larger than in the other spots. The positions go from the inner side to the outer side of the ring, roughly located in East-West direction, with an extension projected on the sky, similar to the ring diameter. These spots are the more intense at the ring. HII regions with a ring shape have been observed at W49N (De Pree et al., 2000). One of them is at the North, out of the field of view of the present plot. Hollenbach et al. (1994) suggest that such UC HII regions may result of photoevaporating circumstellar disks.

5. Estimation of the magnetic field by using Zeeman pairs

The Magnetic field along the line of sight is estimated at locations where two spots of opposite polarization spatially coincide. The errors in the estimations of the spots coordinates are used to determine whether the offset in the coordinates is significant or not. To estimate the magnetic field (B) the next equation is used,

$$B = \frac{\Delta v}{C} \tag{1}$$

where dv is the difference between the velocities and C is a constant that depends on the frequency. The constant is given in $km\ s^{-1}/mG$ and it is 0.122 for 1612 MHz, 0.590 for 1665 MHz and 0.354 for 1667 MHz. The error in estimating the central velocity of a spot with the XGAUSS routine typically is less than 0.01 $km\ s^{-1}$. The largest errors are $\leq 0.03\ km\ s^{-1}$. Therefore, the error in the estimation of the magnetic field is ≤ 0.25 mG for 1612 MHz, ≤ 0.05 mG for 1665 MHz and ≤ 0.08 mG for 1667 MHz. In Table 8 the Zeeman pairs are given. Taking into account the small errors in the estimation of the central velocity, we give the velocities in Tables 8, 9 and 10 with two decimals. The computation of the magnetic field was done based on the velocity difference between such values. We found that, in some cases, the shift in locations is larger than the errors because the orientations of the PA are considerably different. That cases are also listed in Tables 9 and 10 as Zeeman pairs.

5.1. Magnetic field at the small arc

In Fig.5 **a)** the velocity of the LCP (open circles) and RCP (closed circles) 1667 MHz spots located at the small arc are given versus distances. The distances are referenced to the Eastern spot. The difference in velocity between LCP and RCP velocities is due to the local magnetic field (Fish et al. 2006). The six spots form Zeeman pairs whose estimated magnetic field is given at the corresponding pair between the velocities of LCP and RCP spots at the distance of the spots, respect the reference. The magnetic field is nearly constant for the arc with an indication of a smooth gradient (of $\sim 3.3X10^{-4}$ mG/AU) with decreasing strength from East to West.

5.2. Magnetic field at the jet

In Fig.5 **b)** the velocity and distance for the spots located at the jet are shown. Also, the open circles are for LCP and closed circles for RCP 1667 MHz data and the estimated magnetic field is shown between the data of the corresponding pair. Three pairs are found at the jet. It may be seen that the LCP spots at distances from 100 mas to 550 mas may be fitted by a straight line. The RCP spots from 0 mas to 550 mas also may be fitted by a straight line. The velocity difference between the lines fitted is nearly constant with a small increase (in a spatial scale of $\sim$ 700 mas ($\sim$ 8000 AU)). In spite of the fact that not

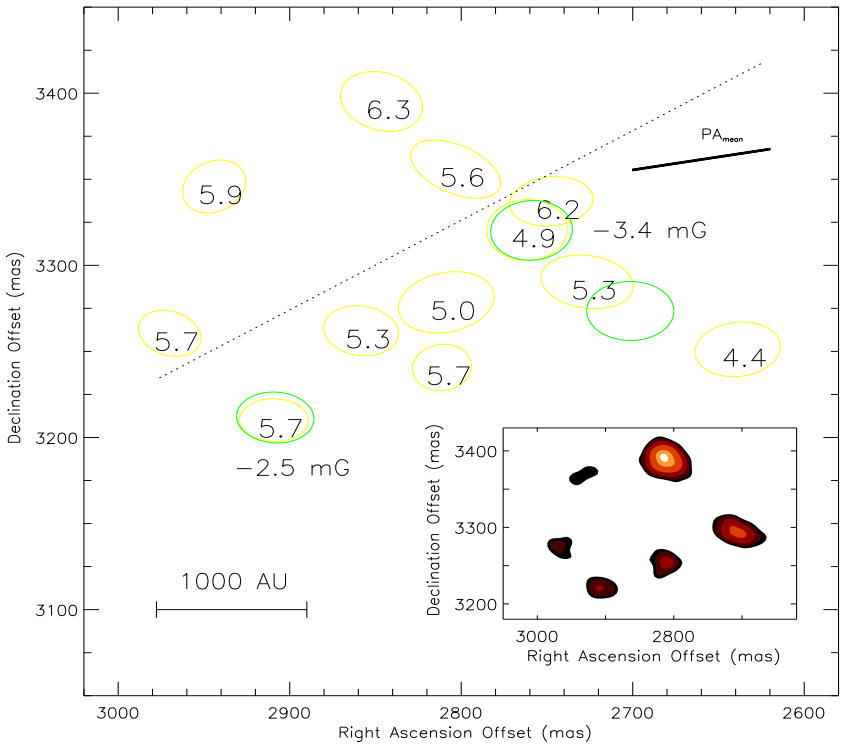

Fig. 4. In the main panel the yellow ellipses denote the LCP spots and the green ellipses the RCP spots observed at 1667 MHz forming a ring at the North-East of the field. Ellipses are of the actual sizes. The orientation and the sizes are as estimated by the JMFIT routine. The dotted line indicates a constant Longitude. The values inside yellow ellipses are the velocities. The values at a side of a spot pair (coincident yellow and blue ellipses) are the estimated magnetic fields. The bar on the right-lower corner indicates the orientation of $PA_{\rm mean}$, the mean value for the 1667 MHz spots. The three northern spots attained the maximum flux at other velocities. The location, the orientation of PA and the Major axis of the bars for these spots correspond to the values at the velocity of maximum flux of each of them. It may be seen that the orientations of the spots with velocities 5.6 km s^{-1} and 5.7 km s^{-1} (at the East) considerably differ from that of constant galactic longitude and from $PA_{\rm mean}$. In the subframe the LCP spots at 5.7 km s^{-1} observed at 1667 MHz are plotted. Not all the spots attained the maximum flux at this velocity.

all the spots fitted by these lines are Zeeman pairs one may to consider that the behavior of the magnetic field accomplish also for the intermediate locations (as if there were spots forming pairs along the straight lines). It is interesting to note that the difference between LCP and RCP velocities decreases at the locations where the maximum velocity is reached. This smaller difference means a weaker magnetic field in this region. According to Fig. 3 further to this point the spots spread by ~ 200 mas (~ 2300 AU). At the reference location there are no RCP spots. However, if we extrapolate the RCP line to the initial location the RCP velocity comes to the same value as the observed LCP velocity, which would correspond to a zero magnetic field at the southernmost location of these set of

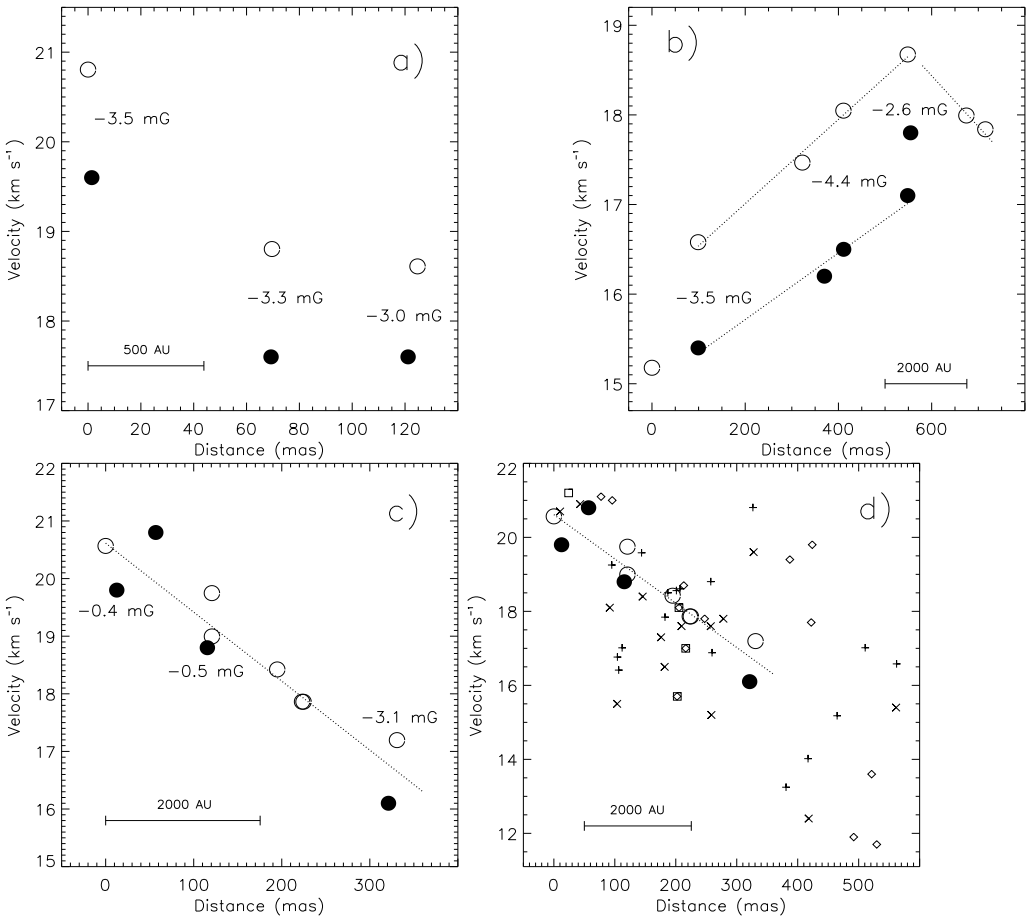

Fig. 5. The velocity as a function of the distance of the spots (open circles denote LCP 1667 MHz data and closed circles RCP 1667 MHz data) at, **a)** the small arc. The distance was measured taking as reference the location of the Easternmost spot. The values given between pairs of LCP and RCP data correspond to the estimated magnetic fields. **b)** the jet (denoted by the vertical straight line of Fig.3), **c)** the large arc, taking into account only the spots that lie at the large circle drawn in Fig.3. **d)** the large arc and the spots with values at the velocity and distance ranges of this plot. The *plus* denote the LCP 1667 MHz data of spots that do not lie at the arc but are at the distances in the range of this plot, the *product* denotes the RCP 1667 MHz data, *rombes* the LCP 1665 MHz data and *squares* the RCP 1665 MHz data .

spots. From 100 mas to 350 mas there is an increasing magnetic field but at the distance of 350 the field decreases. The increasing magnetic field would accelerate charged particles while the decreasing magnetic field would brake down charged particles. This magnetic field could be the origin of the accelerated stream of particles along the jet.

5.3. Magnetic field at the large arc

In Fig.5 **c)** the velocity and distance for the spots at the large arc are plotted. Distances are given respect the southernmost spot. The open circles denote LCP and closed circles the RCP 1667 MHz data. Distances are measured taking as reference the spot at the

South-East of the arc (of those that lie at the large dashed circle). The straight line is fitted for LCP and RCP data together. It may be seen that about the location of the reference spot and at a distance of 300 mas (∼3800 AU) the LCP velocity is smaller than RCP one. However, there are no clear trends for the velocity variations neither for LCP nor for RCP data and there is no a tendency of the velocity difference to be around a given value or have regular variations. Around the region of the spots with magnetic field of -0.5 mG, at a distance of 100 mas (∼1100 AU) there is a Zeeman pair for which the estimated magnetic field is -3.7 mG. At other locations of the backside of the large arc there are some other Zeeman pairs that lead to magnetic fields that differ from those at the arc by few milliGauss. These values and the values at the arc itself, indicate that the magnetic field at the arc and at its back side have large differences even between near locations. This behaviour considerably differs from that of the magnetic field at the small arc and at the jet. In Fig.5 **d)** the data of spots of Fig. 3 is plotted together with those at the region that are not farther than 600 mas (∼ 7000 AU) from the reference spot. It is clear that in this set of spots also is seen a velocity decrease as the distance increases. This could indicate that the spots near to the arc are dynamically related to the arc and to the source that drives it.

5.4. Magnetic field at the ring

A Zeeman pair is observed at the NW of the ring. It leads to a magnetic field estimation of -3.4 milliGauss. At the South of the ring another pair leads to a field of -2.5 milliGauss. The behaviour of the magnetic field at the ring can not be estimated base on these two pairs. However, the fact that the locations of the spots change from one channel to other is indicative of the presence of a magnetic field all around the ring. Since the LCP 1667 MHz spots are weak then RCP 1667 MHz emission probably is even more weak to be detected.

6. Spatial distribution on galactic Coordinates

The distribution of the spots galactic coordinates are shown in Fig.6 and Fig.7. It may be seen that the behaviour differs from each other. The distribution of the Longitudes does not follow a single Gaussian shape neither for a histogram with binning interval of 200 mas (Fig.6) nor for a 500 mas one. Moreover, there are gaps that separate groups of more than ten spots. One of these groups has more that twenty spots. It is as if the groups were clumped at different longitudes. The 1612 MHz spots lie at smaller longitudes than 1665 MHz and 1667 MHz spots. Clearly, the 1612 MHz spots are at Longitudes at an extreme of the 1665 MHz and 1667 MHz distributions. On the other hand, the Galactic Latitude for the spots at the three frequencies are clumped around a mean value of about 42.5 (Fig.7). At the histogram made with a binning interval of 200 mas there are

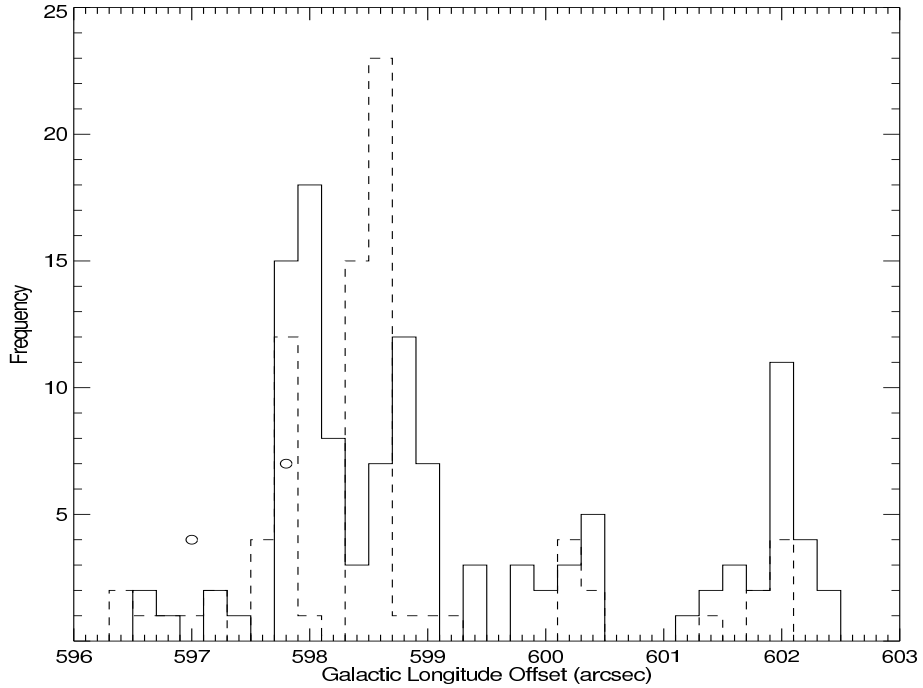

Fig. 6. Number distribution (histogram) of the Galactic Longitude for the 1667 MHz spots (continous line), for the 1665 MHz spots (dashed line) and for the 1612 MHz spots (circles). The Longitude Offset is given respect the galactic center.

no important gaps (the separated groups has less than ten spots). In the histogram made with a binning interval of 300 mas one of these gaps disappears and the remaining groups have five or less spots.

7. Discussion

Velocity gradients have been observed in other OH sources (Fish et al. 2006). However, the velocity gradients at the small arc and at the jet are seen together with magnetic field gradients. A velocity gradient does not necessarily implies a magnetic field gradient since the magnetic field depends on the velocity difference between the two polarization, but not on the value of one of the velocities. The large arc also shows a velocity gradient but the magnetic field seems to be inhomogenous and probably could be the result of turbulence. In this case, the velocity gradients could be explained if the spots are in a velocity field such as a turbulent eddy. However, the size of such an eddy would have to be of the order of 4000 AU. It has been found that the PA takes similar values even for quite separated spots. On the other hand, the PA, major axis and minor axis show clear differences from one frequency to other. Also, a remarkably difference is seen between the Major and minor axes values. The above results indicate that the magnetic field seems to be playing an important role at both the small scale structures and the behaviour of the spots over a large scale. A magnetic field would lead to an anisotropic velocity field (Higdon 1986) that would lead to density anisotropies. The difference between the Major

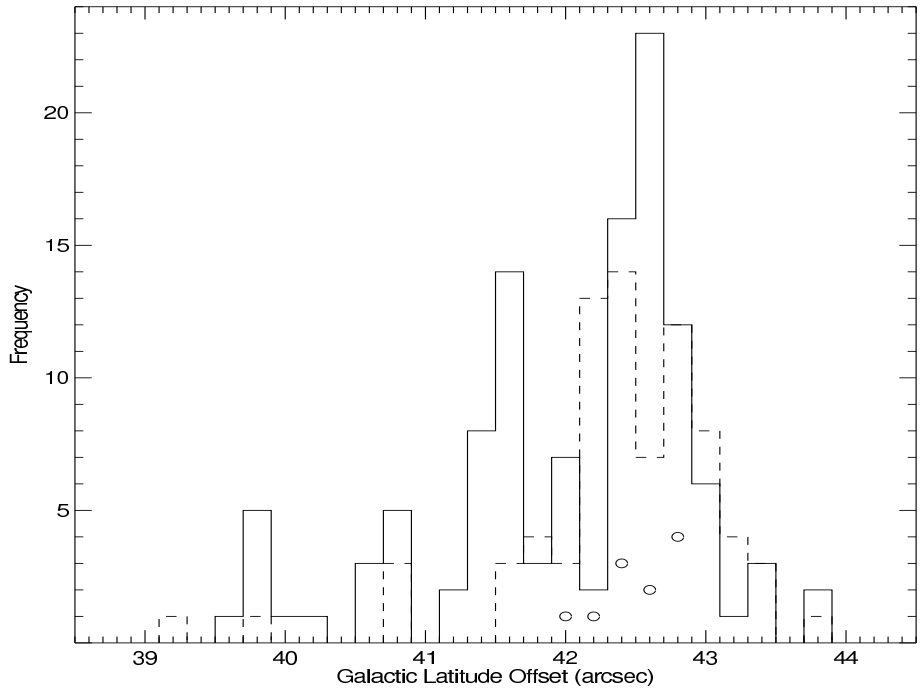

Fig. 7. Histogram of the Galactic Latitude for the 1667 MHz spots (continous line), for the 1665 MHz spots (dashed line) and for the 1612 MHz spots (circles).

and minor axes, in principle could be explained with two different inner length scales of the power spectrum, along and perpendicular to the magnetic field.

8. Conclusions

At the three frequencies more spots at LCP than at RCP were detected. Some structures are outlined by the spots. The magnetic field at some of them could be estimated. For two structures (the small arc and the jet) a velocity and a magnetic field gradient are observed.

Acknowledgements.

References

Armstrong, J. W., Cordes, J. M., and Rickett, B.J. 1981, Nature, 291, 561

Coles, W.A., Frehlich,R.G., Rickett, B., and Codona, J.L. 1987, ApJ, 315, 666

Cordes84 Cordes, J. M.,Ananthakrishnan, S., and Dennison, B. 1984, Nature,309,689

Fish, V.L., Brisken, W.F, Sjouwerman, L.O. 2006, ApJ, 647, 418

Gwinn, C.R., Bartel, N., and Cordes, J.M. 1993, ApJ, 410, 673

Gwinn, C.R., Moran, J.M., Reid, M. 1992, ApJ, 393, 149

Kent, S. R. Mutel R. L. 1982, ApJ 263, 145

Diamond, P. J., Martison, A., Booth, R. S., Winnberg, A. 1988, Radio Wave Scattering in the Interstellar Medium, AIP Conference Proceedings 174, New York, AIP, p. 195

Higdon, J.C. 1986, ApJ, 309, 342

Moran, J. M., Rodriguez, L. F., Greene, B., Backer, D.C. 1990, ApJ, 348, 174

Narayan, R., Hubbard, W.B. 1988, ApJ, 325, 503

Rickett, B.J., Coles, W. A., Bourgois, G. 1984, A&A, 134,390

Rickett, B.J. 1990, ARA&A, 28, 561

Shebalin, J. V., Matthaeus, W. H., Montgomery, D. 1983, J. Plasma Phys., 29, 525

Silant'ev, N.A., Lekht, E.E., Mendoza-Torres, J.E., Rudnitskij, G.M. 2006, A&A, 453, 989

Taylor, J.H. Cordes, J.M. 1993, ApJ, 411, 674

9. Appendix A

Table 2. W49N 1612 MHz LCP Maser Parameters

Feature	Vel (km s^{-1})	Width (km s^{-1})	Peak (Jy $Beam^{-1}$)	$\Delta\alpha$ (mas)	$\Delta\delta$ (mas)	PA (Degrees)
1.....	20.6	0.6	0.2	-596.2	-590.0	170.3
2.....	16.5	1.1	0.1	-180.6	100.9	172.3
3.....	16.0	0.8	0.1	-29.0	-893.9	164.6
4.....	15.0	0.5	2.7	-9.5	15.1	170.6
5.....	14.1	0.5	2.4	-0.7	0.8	166.3
6.....	13.4	0.6	0.2	18.5	-33.3	174.2

Table 3. W49N 1612 MHz RCP Maser Parameters

Feature	Vel (km s^{-1})	Width (km s^{-1})	Peak (Jy $Beam^{-1}$)	$\Delta\alpha$ (mas)	$\Delta\delta$ (mas)	PA (Degrees)
1.....	18.9	0.6	0.2	-582.5	-594.4	119.2
2.....	17.1	0.8	0.1	-185.9	105.6	108.0
3.....	15.7	0.7	1.8	-9.4	15.2	115.3
4.....	14.8	0.5	7.8	0.0	0.1	107.5
5.....	14.1	0.5	0.4	19.5	-34.7	125.5

.

Table 4. W49N 1665 MHz LCP Maser Parameters

Feature	Vel	Width	Peak	$\Delta\alpha$	$\Delta\delta$	PA
	(km s^{-1})	(km s^{-1})	(Jy Beam^{-1})	(mas)	(mas)	(Degrees)
1.....	21.1	0.4	4.9	45.7	25.3	164.7
2.....	21.0	0.4	40.6	-0.5	-0.3	168.7
3.....	20.3	0.3	0.4	-929.5	-1107.7	161.5
4.....	19.8	0.4	1.0	105.0	-318.7	170.2
5.....	19.7	0.5	0.5	-52.3	798.1	173.6
6.....	19.6	0.5	0.5	-92.8	900.0	156.8
7.....	19.6	0.4	0.5	-143.2	935.3	10.5
8.....	19.4	0.5	0.1	155.3	-750.2	156.5
9.....	19.3	0.6	0.3	537.1	1138.0	165.7
10.....	19.3	0.4	1.0	-360.4	-13.0	170.4
11.....	18.7	0.5	0.9	-22.4	738.7	101.7
12.....	18.8	0.8	2.4	179.8	-35.9	167.7
13.....	18.3	0.4	20.0	-26.5	720.7	171.0
14.....	18.1	0.5	10.5	175.5	-28.7	169.7
15.....	17.7	0.3	1.0	557.3	1182.6	166.6
16.....	17.7	0.6	0.5	173.2	-89.9	173.0
17.....	17.7	0.5	0.5	-378.0	-68.4	170.3
18.....	17.6	0.6	2.9	-51.6	745.2	170.2
19.....	16.9	0.6	24.6	176.7	-44.9	166.1
20.....	15.8	0.6	15.1	173.0	-27.3	168.9
21.....	15.7	0.5	6.5	-5.4	839.9	174.9
22.....	15.1	0.8	0.7	985.7	443.9	165.1
23.....	14.6	0.4	2.6	585.4	433.8	170.0
24.....	14.2	0.4	0.2	-1286.6	-477.7	171.3
25.....	13.8	0.4	4.1	987.1	2069.3	172.6
26.....	13.6	0.6	0.5	388.4	455.4	165.6
27.....	13.2	0.5	0.2	-329.1	903.2	163.9
28.....	12.1	0.5	16.9	954.0	2196.7	168.9
29.....	11.9	0.4	1.2	292.7	498.2	170.9
30.....	11.8	0.7	1.8	623.2	569.5	176.4
31.....	11.7	0.3	3.9	287.8	546.5	170.2
32.....	11.1	0.5	5.2	655.2	462.2	166.6
33.....	9.4	0.5	3.9	676.1	481.0	171.0
34.....	8.2	0.6	2.3	880.2	410.4	168.9
35.....	7.8	0.5	1.1	653.4	456.8	174.6
36.....	5.7	0.7	1.1	3356.3	2617.2	173.5
37.....	5.2	0.5	3.5	2808.4	3286.1	153.6
38.....	5.0	0.9	1.0	3365.3	2650.7	162.3
39.....	4.8	0.4	1.2	2675.5	3259.4	158.2
40.....	4.1	0.6	0.2	676.8	348.7	173.0

.

Table 5. W49N 1665 MHz RCP Maser Parameters

Feature	Vel	Width	Peak	$\Delta\alpha$	$\Delta\delta$	PA
	(km s^{-1})	(km s^{-1})	(Jy Beam^{-1})	(mas)	(mas)	(Degrees)
1.....	21.2	0.4	0.7	14.4	118.8	110.7
2.....	20.0	0.5	2.1	-36.1	727.9	110.5
3.....	19.5	0.3	5.7	-138.4	932.8	109.0
4.....	18.5	0.6	0.6	-548.3	909.0	110.6
5.....	18.2	0.4	0.8	-12.2	848.9	119.2
6.....	18.2	0.5	14.0	175.5	-28.6	104.7
7.....	17.5	0.5	2.8	-51.9	746.3	108.7
8.....	17.0	0.5	27.6	179.0	-42.0	102.0
9.....	16.3	0.5	1.3	-28.5	894.6	119.0
10.....	16.3	0.5	0.8	-24.0	929.9	112.6
11.....	15.8	0.5	20.8	173.2	-27.0	105.5
12.....	15.3	0.4	2.3	-51.3	889.9	109.6
13.....	15.1	0.4	7.2	-966.6	179.6	107.0
14.....	14.8	0.4	0.3	-209.3	757.1	107.3
15.....	14.7	0.4	0.9	-344.0	776.2	110.8
16.....	14.0	0.4	0.6	-337.9	822.2	105.4
17.....	13.3	0.4	1.1	-1384.2	50.0	108.6
18.....	13.0	0.4	1.8	-1161.4	-751.3	107.8
19.....	13.1	0.5	0.3	-698.0	-532.8	112.5
20.....	12.6	0.4	0.8	990.7	453.2	104.8
21.....	12.3	0.4	0.7	952.9	2188.4	113.2
22.....	12.1	0.5	0.3	624.6	560.5	101.2
23.....	11.9	0.4	1.1	869.8	2462.4	110.2
24.....	11.2	0.5	1.3	655.2	460.8	104.6
25.....	10.9	0.5	3.1	585.7	435.6	107.8
26.....	10.4	0.4	4.7	872.6	704.9	120.1
27.....	9.9	0.4	0.5	990.4	2048.0	120.4
28.....	9.4	0.5	0.8	635.0	475.2	111.2
29.....	8.3	0.6	0.4	623.5	560.2	113.8
30.....	7.8	0.5	3.1	654.8	456.1	110.9
31.....	7.7	0.4	1.7	895.7	414.7	100.9
32.....	6.4	0.8	0.3	3458.5	-3467.9	77.6
33.....	5.7	0.4	0.5	678.2	482.0	109.9
34.....	3.6	0.4	0.7	2812.7	3278.5	100.5
35.....	1.1	0.4	0.3	2844.0	-1603.4	98.7

Table 6. W49N 1667 MHz LCP Maser Parameters

Feature	Vel	Width	Peak	$\Delta\alpha$	$\Delta\delta$	PA
	(km s^{-1})	(km s^{-1})	(Jy Beam^{-1})	(mas)	(mas)	(Degrees)
1.....	20.8	0.4	0.7	313.2	219.3	161.3
2.....	20.6	0.5	0.8	11.9	93.1	14.1
3.....	20.3	0.5	0.5	-46.4	1106.3	150.1
4.....	19.7	0.7	2.2	-70.2	183.6	169.2
5.....	19.6	0.3	0.4	-58.3	-28.8	131.2
6.....	19.3	0.6	7.8	-0.2	0.4	156.6
7.....	19.0	0.4	12.1	-67.8	185.8	159.8
8.....	18.8	0.3	0.8	252.0	186.0	153.3
9.....	18.6	0.4	0.4	187.9	201.2	177.4
10.....	18.7	0.6	0.2	351.0	988.6	167.9
11.....	18.6	0.5	0.3	120.1	-74.4	136.7
12.....	18.5	0.4	0.7	136.6	-44.2	159.8
13.....	18.4	0.5	2.2	-95.4	256.1	164.5
14.....	18.0	0.5	0.1	300.0	1118.2	170.2
15.....	18.0	0.6	0.5	314.3	850.7	159.4
16.....	17.8	0.4	0.2	482.8	1137.2	153.1
17.....	17.9	0.6	0.6	-93.0	291.8	157.1
18.....	17.8	0.9	1.2	137.3	-37.4	156.8
19.....	17.9	0.6	0.6	-92.7	292.0	145.0
20.....	17.8	0.6	0.3	-1422.4	34.0	162.2
21.....	17.6	0.7	0.1	-2164.0	2408.4	148.8
22.....	17.5	0.3	0.1	343.9	764.3	144.5
23.....	17.2	0.8	0.1	-64.8	418.0	149.5
24.....	17.0	0.4	0.1	-454.0	320.2	176.5
25.....	17.0	0.4	0.1	-38.1	-5.5	160.4
26.....	16.9	0.4	1.2	-2244.2	2358.0	161.9
27.....	16.9	0.4	0.6	-231.4	10.5	152.8
28.....	16.8	0.5	1.2	-86.6	128.7	156.4
29.....	16.6	0.7	0.3	373.0	525.2	152.1
30.....	16.4	0.7	0.2	-31.4	-2.3	150.9
31.....	16.3	0.4	0.3	-2219.0	2322.0	172.8
32.....	15.8	0.5	0.9	886.0	2192.4	157.8
33.....	15.6	0.8	0.4	896.0	2189.9	157.3
34.....	15.6	0.4	0.1	-1095.5	-3.5	154.0
35.....	15.4	0.6	0.3	-2194.9	2400.5	133.1
36.....	15.2	0.8	0.1	322.3	439.6	154.2
37.....	14.8	0.5	0.7	952.2	443.5	157.5
38.....	14.5	0.6	0.7	-1316.5	-494.6	166.8
39.....	14.0	0.4	1.1	-336.6	324.4	166.4
40.....	13.4	0.6	0.7	1247.4	679.3	162.4

Table 7. W49N 1667 MHz RCP Maser Parameters

Feature	Vel (km s^{-1})	Width (km s^{-1})	Peak (Jy $Beam^{-1}$)	$\Delta\alpha$ (mas)	$\Delta\delta$ (mas)	PA (Degrees)
1.....	20.9	0.3	0.4	-5.4	55.8	160.6
2.....	20.8	0.5	0.3	-38.1	122.8	156.5
3.....	20.7	0.5	0.2	7.0	85.5	163.7
4.....	19.8	0.6	0.4	5.7	107.3	170.8
5.....	19.6	0.4	0.8	314.6	219.1	160.5
6.....	18.8	0.7	0.1	-68.0	178.5	139.4
7.....	18.5	0.4	0.5	-2243.2	2356.9	162.0
8.....	18.4	0.6	0.3	-61.6	-31.4	160.3
9.....	18.2	0.7	0.6	3.5	3.7	150.9
10.....	17.7	0.4	1.0	-174.5	301.6	161.0
11.....	17.7	0.5	0.2	250.2	191.6	162.6
12.....	17.6	0.5	0.5	363.2	994.0	161.6
13.....	17.6	0.3	0.2	194.0	196.9	160.3
14.....	17.3	0.6	0.8	127.4	-37.5	169.9
15.....	17.1	0.4	1.0	355.4	987.8	158.9
16.....	16.5	0.6	0.8	314.0	851.4	157.7
17.....	16.5	0.4	0.5	136.9	-36.8	160.2
18.....	16.2	0.4	0.2	369.7	807.1	144.4
19.....	16.1	0.4	0.4	-67.3	406.1	158.4
20.....	15.5	0.4	2.8	-86.5	128.8	159.4
21.....	15.3	0.5	0.2	367.6	530.3	157.5
22.....	15.2	0.5	0.3	-231.7	10.4	151.2
23.....	14.3	0.4	1.8	-1423.8	36.0	158.0
24.....	13.7	0.4	0.5	887.4	2193.1	152.1
25.....	13.6	0.5	0.5	-1258.6	-673.6	164.0
26.....	13.2	0.4	1.0	954.0	443.9	158.1
27.....	12.4	0.4	1.1	-336.9	325.9	164.4
28.....	11.6	0.6	1.0	920.2	767.5	161.3
29.....	10.4	0.4	0.3	844.2	689.0	168.1
30.....	9.5	0.6	0.2	578.2	549.4	170.5
31.....	8.7	0.4	0.6	896.0	2462.8	160.5
32.....	8.3	0.4	0.6	865.1	420.1	154.3
33.....	7.9	0.5	0.3	3186.7	3494.9	145.9
34.....	7.6	0.5	0.2	2208.2	1679.8	150.5
35.....	6.4	0.4	0.1	2201.8	538.2	162.2
36.....	6.4	0.5	0.2	2241.7	580.7	145.8
37.....	5.6	0.8	0.4	3296.2	532.8	153.8
38.....	4.9	0.5	0.3	3884.4	2557.8	163.8
39.....	4.7	0.6	0.2	3322.1	2602.8	133.0
40.....	4.7	0.5	0.3	2908.8	3211.6	148.6

Table 8. W49N 1612 MHz LCP Zeeman pairs

Vel	α off	σ	δ off	σ	Vel	α off	σ	δ off	σ	$\Delta\alpha$	$\sigma(\alpha)$	$\Delta\delta$	$\sigma(\delta)$	B
(kms^{-1})	(mas)	(mas)	(mas)	(mas)	(kms^{-1})	(mas)	(mas)	(mas)	(mas)	(mas)	(mas)	(mas)	(mas)	mG
	RCP	1612					LCP				RCP	LCP		
18.85	-582.5	1.0	-594.4	0.9	20.57	-596.2	1.6	-590.0	1.1	13.7	1.9	4.4	1.4	-14.08
17.13	-185.9	2.0	105.6	1.5	16.46	-180.6	3.1	100.9	1.9	5.3	3.7	4.7	2.4	5.54
15.70	-9.4	0.2	15.2	0.1	15.00	-9.5	0.1	15.1	0.1	0.1	0.2	0.1	0.1	5.78
14.76	0.0	0.0	0.1	0.0	14.06	-0.7	0.1	0.8	0.1	0.7	0.1	0.7	0.1	5.79

Table 9. W49N 1665 MHz LCP Zeeman pairs

Vel	α off	σ	δ off	σ	Vel	α off	σ	δ off	σ	$\Delta\alpha$	$\sigma(\alpha)$	$\Delta\delta$	$\sigma(\delta)$	B
(kms^{-1})	(mas)	(mas)	(mas)	(mas)	(kms^{-1})	(mas)	(mas)	(mas)	(mas)	(mas)	(mas)	(mas)	(mas)	mG
	RCP	1665					LCP				RCP	LCP		
19.51	-138.4	0.1	932.8	0.0	19.55	-143.2	0.6	935.3	0.5	4.8	0.6	2.5	0.5	-0.07
17.54	-51.9	0.1	746.3	0.1	17.56	-51.6	0.1	745.2	0.1	0.3	0.1	1.1	0.1	-0.03
18.21	-12.2	0.5	848.9	0.4	15.66	-5.4	0.1	839.9	0.0	6.8	0.5	9.0	0.4	4.31
10.90	585.7	0.1	435.6	0.1	14.62	585.4	0.1	433.8	0.1	0.3	0.1	1.8	0.1	-6.30
12.27	952.9	0.4	2188.4	0.3	12.09	954.0	0.0	2196.7	0.0	1.1	0.4	8.3	0.3	0.30
12.08	624.6	0.8	560.5	0.6	11.77	623.2	0.2	569.5	0.1	1.4	0.8	9.0	0.6	0.52
8.28	623.5	0.4	560.2	0.4	11.77	623.2	0.2	569.5	0.1	0.3	0.4	9.3	0.4	-5.92
11.21	655.2	0.2	460.8	0.1	11.12	655.2	0.1	462.2	0.0	0.0	0.2	1.4	0.1	0.16
5.67	678.2	0.4	482.0	0.3	9.37	676.1	0.1	481.0	0.0	2.1	0.4	1.0	0.3	-6.27
11.21	655.2	0.2	460.8	0.1	7.78	653.4	0.2	456.8	0.2	1.8	0.3	4.0	0.2	5.81
7.79	654.8	0.1	456.1	0.1	7.78	653.4	0.2	456.8	0.2	1.4	0.2	0.7	0.2	0.01
3.58	2812.7	0.4	3278.5	0.3	5.21	2808.4	0.1	3286.1	0.1	4.3	0.4	7.6	0.3	-2.77

Table 10. W49N 1667 MHz LCP Zeeman pairs

Vel	α off	σ	δ off	σ	Vel	α off	σ	δ off	σ	$\Delta\alpha$	$\sigma(\alpha)$	$\Delta\delta$	$\sigma(\delta)$	B
(kms^{-1})	(mas)	(mas)	(mas)	(mas)	(kms^{-1})	(mas)	(mas)	(mas)	(mas)	(mas)	(mas)	(mas)	(mas)	mG
	RCP	1667					LCP				RCP	LCP		
19.58	314.6	0.3	219.1	0.2	20.81	313.2	0.5	219.3	0.3	1.4	0.6	0.2	0.4	-3.46
20.71	7.0	1.2	85.5	0.9	20.57	11.9	0.4	93.1	0.3	4.9	1.3	7.6	0.9	0.41
19.81	5.7	0.7	107.3	0.5	20.57	11.9	0.4	93.1	0.3	6.2	0.8	14.2	0.6	-2.14
18.84	-68.0	1.4	178.5	1.2	19.75	-70.2	0.1	183.6	0.1	2.2	1.4	5.1	1.2	-2.58
18.35	-61.6	0.8	-31.4	0.5	19.58	-58.3	0.6	-28.8	0.4	3.3	1.0	2.6	0.6	-3.48
18.21	3.5	0.5	3.7	0.3	19.25	-0.2	0.0	0.4	0.0	3.7	0.5	3.3	0.3	-2.94
18.84	-68.0	1.4	178.5	1.2	19.00	-67.8	0.0	185.8	0.0	0.2	1.4	7.3	1.2	-0.45
17.73	250.2	1.1	191.6	0.9	18.80	252.0	0.4	186.0	0.3	1.8	1.2	5.6	0.9	-3.03
17.63	194.0	0.9	196.9	0.7	18.61	187.9	0.8	201.2	0.6	6.1	1.2	4.3	0.9	-2.76
17.62	363.2	0.6	994.0	0.3	18.67	351.0	1.1	988.6	0.9	12.2	1.3	5.4	0.9	-2.98
17.06	355.4	0.3	987.8	0.2	18.67	351.0	1.1	988.6	0.9	4.4	1.1	0.8	0.9	-4.55
17.34	127.4	0.4	-37.5	0.3	18.50	136.6	0.4	-44.2	0.3	9.2	0.6	6.7	0.4	-3.28
16.50	136.9	0.5	-36.8	0.3	18.50	136.6	0.4	-44.2	0.3	0.3	0.6	7.4	0.4	-5.65
16.53	314.0	0.3	851.4	0.2	17.99	314.3	0.5	850.7	0.3	0.3	0.6	0.7	0.4	-4.14
17.34	127.4	0.4	-37.5	0.3	17.84	137.3	0.2	-37.4	0.1	9.9	0.4	0.1	0.3	-1.43
16.50	136.9	0.5	-36.8	0.3	17.84	137.3	0.2	-37.4	0.1	0.4	0.5	0.6	0.3	-3.79
14.30	-1423.8	0.1	36.0	0.1	17.76	-1422.4	0.8	34.0	0.5	1.4	0.8	2.0	0.5	-9.79
16.20	369.7	1.1	807.1	0.8	17.47	343.9	2.3	764.3	1.6	25.8	2.5	42.8	1.8	-3.59
16.12	-67.3	0.6	406.1	0.4	17.20	-64.8	2.9	418.0	1.6	2.5	3.0	11.9	1.6	-3.05
18.35	-61.6	0.8	-31.4	0.5	17.01	-38.1	2.3	-5.5	1.5	23.5	2.4	25.9	1.6	3.77
18.21	3.5	0.5	3.7	0.3	17.01	-38.1	2.3	-5.5	1.5	41.6	2.4	9.2	1.5	3.38
18.53	-2243.2	0.5	2356.9	0.4	16.91	-2244.2	0.2	2358.0	0.2	1.0	0.5	1.1	0.4	4.59
15.21	-231.7	0.6	10.4	0.5	16.88	-231.4	0.4	10.5	0.3	0.3	0.7	0.1	0.6	-4.73
15.47	-86.5	0.1	128.8	0.1	16.76	-86.6	0.2	128.7	0.1	0.1	0.2	0.1	0.1	-3.67
15.35	367.6	1.1	530.3	0.8	16.58	373.0	0.8	525.2	0.5	5.4	1.4	5.1	0.9	-3.47
18.21	3.5	0.5	3.7	0.3	16.41	-31.4	1.7	-2.3	0.7	34.9	1.8	6.0	0.8	5.08
13.67	887.4	0.4	2193.1	0.3	15.81	886.0	0.3	2192.4	0.2	1.4	0.5	0.7	0.4	-6.05
13.67	887.4	0.4	2193.1	0.3	15.62	896.0	0.6	2189.9	0.4	8.6	0.7	3.2	0.5	-5.52
13.22	954.0	0.3	443.9	0.2	14.77	952.2	0.4	443.5	0.2	1.8	0.5	0.4	0.3	-4.40
12.36	-336.9	0.2	325.9	0.2	14.02	-336.6	0.2	324.4	0.2	0.3	0.3	1.5	0.3	-4.67
13.60	-1258.6	0.5	-673.6	0.3	13.44	-1247.4	0.4	-679.3	0.3	11.2	0.6	5.7	0.4	0.43
11.60	920.2	0.3	767.5	0.2	12.55	925.2	3.8	758.9	1.2	5.0	3.8	8.6	1.2	-2.69
11.60	920.2	0.3	767.5	0.2	12.17	910.1	1.9	766.1	1.0	10.1	1.9	1.4	1.0	-1.62
9.48	578.2	0.9	549.4	0.7	11.21	589.3	0.7	554.8	0.5	11.1	1.1	5.4	0.9	-4.88
10.39	844.2	0.8	689.0	0.6	10.51	836.6	1.0	703.4	1.2	7.6	1.3	14.4	1.3	-0.33
8.27	865.1	0.5	420.1	0.3	8.26	861.5	2.8	420.5	1.8	3.6	2.8	0.4	1.8	0.01
7.59	2208.2	1.0	1679.8	0.7	8.23	2208.2	1.9	1682.3	1.3	0.0	2.1	2.5	1.5	-1.82
6.44	2201.8	3.7	538.2	1.7	7.95	2246.0	1.1	580.0	0.7	44.2	3.9	41.8	1.8	-4.27